GLASS MELTING AND ITS INNOVATION POTENTIALS: THE IMPACT OF THE INPUT AND OUTPUT GEOMETRIES ON THE UTILIZATION OF THE MELTING SPACE

MIROSLAV POLÁK, LUBOMÍR NĚMEC

Institute of Chemical Technology Prague, Faculty of Chemical Technology, Laboratory of Inorganic Materials, Technická 5, 166 28 Prague 6, Institute of Inorganic Chemistry of the AS CR, v.v.i., 250 68 Husinec-Řež

E-mail: polakm@vscht.cz

Submitted April 28, 2010; accepted July 9, 2010

Keywords: Space utilization, Sand dissolution, Bubble removal, Space geometry

This work deals with the relation between the input and output geometries of the model melting channel and its space utilization. Space-utilization value was acquired by using the values of the dead spaces for sand dissolution and bubble removal as calculated from the mathematical modeling of both processes. The defined temperature gradients (taken from previous works) were applied and their influence on the melt flow and space utilization was studied. The previously applied simple channel with a full-size frontal entrance and exit was chosen as the reference geometry. All of the cases investigated in this work were conducted under the same conditions with a mean temperature of 1450°C. The isothermal case was selected as the reference case, and the pure transversal gradient and combination of the transversal with the small longitudinal temperature gradients were applied. The results have shown that space utilization is influenced by the input and output geometries of the channel, but the main tendencies resulting from the reference channel with a full-size frontal input and output have been preserved. The aim of this work is to evaluate the best input and output geometries of the melting space for future investigations and practical application.

INTRODUCTION

Glass melting is a physical and chemical process which occurs at high temperatures and in very viscous melts so it consumes a lot of energy and time. To achieve substantial progress in glass making, apparent changes in the process principles, followed by changes of the technological devices, are needed. The problem of high energy consumption is mostly accompanied by high emissions of CO_2, and the low rate of the processes leads to large and expensive melting devices. It is thus desirable to resolve these problems.

The significant role of the space utilisation in melting processes in glass furnaces is known in terms of the the fraction of dead space and the spectrum of melt-residence times in the melting furnace [1]. The high fraction of dead space arises from the circulation regions and regions with lazy flow and the broad spectrum of melt-residence times in the space is caused by the quality differences of single homogenization trajectories. Beerkens declares [2] that the minimum residence time is typically only 15 to 20 % of the average residence time. The spaces without circulation patterns are generally considered most advantageous and spaces - either horizontal [3] or vertical [4] - are proposed for the process to avoid circulations. However, other works [5] and patents utilize the convective circulation currents to raise the molten glass to the surface and aid fining [6-9]. Consequently, there is no clear evidence which spaces and which flow patterns should exhibit a high fining performance .

The newly introduced quantity called utilization of the melting space may help describe the efficiency of the continuous glass-melting space. The basic dependence of the introduced quantity on the character of glass flow in the model channel (resulting from the temperature gradient applied) has already been demonstrated in previous works [10-14]. The aim of the present work is to explore the dependence of space utilization on the geometries of the channel input and output under the same temperature conditions as in the above-mentioned works.

THEORETICAL

The glass-melting process may be described by two significant technological criteria, namely the specific energy consumption and the volume-melting performance. For the isothermal process without energy recycling, both quantities are given by Equations (1) and (2):

$$H_M^0 = H_M^T + \frac{\dot{H}^L \tau_G}{\rho V} = H_M^T + \frac{\dot{H}^L \tau_H}{\rho V}\frac{1}{u} \qquad (1a,b)$$

$$\dot{V} = \frac{V}{\tau_G} = \frac{V}{\tau_H} u \qquad (2a,b)$$

where H_M^0 is the specific energy consumption in Jkg^{-1}; H_M^T is the specific theoretical heat necessary for the chemical reactions, phase transitions and heating of both the batch and melt to the melting temperature T (in Jkg^{-1}); $\dot{H}^L$ is the total heat flux across the space boundary in Js^{-1}; τ_H is the reference homogenization time in s; ρ is the glass density in kg/m^3; V is the space volume in m^3; is the volume flow rate of the melt through the space on the condition that all of the inhomogeneities are removed in m^3s^{-1}; τ_G is the mean residence time of the glass in the space ($\tau_G = V/\dot{V}$).

In the equations above, u is a new quantity which integrally describes the space distribution of the dissolution and bubble removal processes in the melting unit or, in other words, expresses the *space utilization* for the given processes. The space utilization is basically defined as the ratio between the actual process duration in a quiescent glass (obtained from laboratory melts or by calculation from the appropriate kinetic equation) and the mean residence time of glass in the space.

The influence of process kinetics is then involved in the denumerator and the character of the melt flow in the denominator of Equation (3):

$$u = \frac{\tau_H}{\tau_G}\ ; \quad \mathrm{u} \in \langle 0; 1 \rangle \qquad (3)$$

According to Equations (1) and (2), the specific energy consumption decreases and the volume-melting performance increases with increasing space utilization. It is therefore worth examining potential ways that lead to an enhancement of space utilization.

Now, an appropriate classification of the glass-melting process is needed. The homogenization of the glass melt may be generally described by two main processes - the dissolution of solid and liquid inhomogeneities and the separation of gas inhomogeneities (refining). Consequently, space utilization should be defined separately for each process.

The partial quantities, providing a direct relation between the character of the glass flow and the space utilization have been defined as well by the latest works [10-14] as follows: m_G as a fraction of the dead space for glass flow, m_D as a fraction of the dead space for dissolution, m_{virt} as a fraction of the virtual dead space for bubble removal and h_{virt} as a vertical distance that the bubble should overcome in reference to the flowing melt when it rises to the level. The space utilization is then computed by modeling the mentioned partial quantities. The laboratory values of the bubble growth rates and the values characterizing the rate of sand dissolution are also needed to execute the calculations. The relation between the space utilization and the mentioned partial quantities is given by the following two equations [12-13]:

$$u_D = (1 - m_G)\,(1 - m_D) \qquad (4)$$

$$u_F = (1 - m_{virt})\,(h_0 / h_{virt})^{1/3} \qquad (5)$$

where u_D and u_{virt} are the space utilization for dissolution and fining, respectively, and h_0 is the thickness of the glass layer in the space. Equation (4) involves the dissolution of only small inhomogeneities.

Mathematical modeling revealed that different dead spaces and the resulting space utilization itself depend significantly on the type of melt flow, which is evoked by the temperature gradients. The beneficial glass-flow types may then be defined along with the corresponding temperature boundary conditions. Even though the results were acquired by modeling the simple horizontal melting channel with full-size frontal input and output, the validity of the main tendencies is assumed when changing the input and output geometries. This assumption should nevertheless be proven by the further modeling results presented in this work.

Calculation conditions

A horizontal open channel with the following inner dimensions was selected as the model space: the length l_0 = 1.0 m, the width w_0 = 0.5 m and the height of the glass layer h_0 = 0.5 m. The reference glass-melt input and output occupied the entire front walls of 0.5x0.5 m, but the influence of the different input and output geometries was investigated in the following calculations. The examined inputs and outputs thus varied from a half size to a quarter size of the entry or exit walls, whereas their width, equivalent to the channel width (0.5 m), remained preserved in all of the calculations. In the front and back sides, the input or output was designed as close either to the melt level or to the space bottom. One examined variant involved also an inflow by the initial part of the melt level. The glass for the production of TV panels was chosen as the model glass because of the availability of the experimental data. The temperature dependence of the bubble growth rate (needed for bubble modeling) was given by the empirical equation in [12]:

$$\dot{a} = \exp[18.969 - 58554 / (t + 273.15)]\ \ (\mathrm{m/s}); \qquad (6),$$

where t (°C) = <1350; 1550>.

The small bubble (with an initial radius of 5×10^{-5} m) was chosen as the critical one. Its critical trajectory was characterized by the fact that the bubble reached the surface of the glass melt exactly at the end of the channel. The experimentally measured time for the dissolution of sand at 1450 °C was determined to be 1970 s. The temperature dependence of the sand dissolution rate due to temperature differences along the sand particle trajectory has been neglected. Thus, the mentioned dissolution value was also taken as the time of sand dissolution along an arbitrary trajectory [13]. The critical state was indicated by the dissolution of sand on the fastest trajectory just at the channel output. The conditions were thus the same as in the previous works [12-14]. The average residence time of the glass melt in the space, τ, as well as its mean residence time, τ_G, and the sand dissolution time were used to calculate the space utilization for the sand dissolution. The residence time of the critical bubble in the space, τ_F, the mean melt residence time, τ_G, and the reference bubble-fining time, $\tau_{F\mathrm{Ref}}$, (the bubble fining time in a quiescent glass having the same thickness as the layer in the space) were applied to calculate the space utilization for the bubble-removal process.

The appropriate linear temperature gradients, put on the glass level, determined the temperature boundary conditions. Three different types of temperature distributions, which caused different types of glass flow, were examined: isothermal conditions (no circulations), a pure linear transversal temperature gradient of 25°C/m (evoking transverse melt circulations) and the combination of the transversal gradient of 25°C/m with a weak linear longitudinal gradient of 5°C/m (for sand dissolution) or 4°C/m (for bubble removal). The last cases of the combined temperature gradients showed predominantly transverse circulations and corresponded to the best flow arrangement achieved in the previous work [12-14]. The following marks, characterizing the temperature boundary conditions and taken from previous works, were used: ◄ for the longitudinal temperature gradient with a higher output temperature (that is a positive gradient according to the orientation of the x axis), ► for the gradient with a higher input temperature (a negative gradient) and ↕ for the transversal temperature gradient. Hence, the combination <◄5;↕25> designates the case characterized by the combination of the linear longitudinal positive temperature gradient of 5°C/m and the linear transversal gradient of 25°C/m.

The different combinations of the top inputs from the front wall or from the glass level and the top or bottom outputs from the back wall were then examined, i.e. a total of fourteen cases. Special symbols were used to describe briefly and simply the input and output geometries in each case. The symbol ↑ was used for the upper front input or output, the mark ↓ for the bottom one, the level input was designated by *lev.* and the exceptionally used input and output in the middle of the channel height was marked by *mid.* The half-size input and output were designated by ½ and, similarly, the quarter size by ¼. The open channel with full-size input and output, which was explored in previous works [12-14], was chosen as the reference geometry.

The temperature and velocity distributions were calculated by the GS Glass Furnace Model [15]. One thousand bubbles were put into the initial position (the input boundary condition), which passed through the channel *to the target positions at the output*. As for the sand dissolution, one million massless points were examined. Their starting and target positions were the same as for the bubbles.

RESULTS OF THE CALCULATIONS

The following figures show the results of the modeling. The lines between the calculated points are only to guide the eyes, without there being any direct continuity between the individual calculation points. All the figures are labeled in the way already mentioned above.

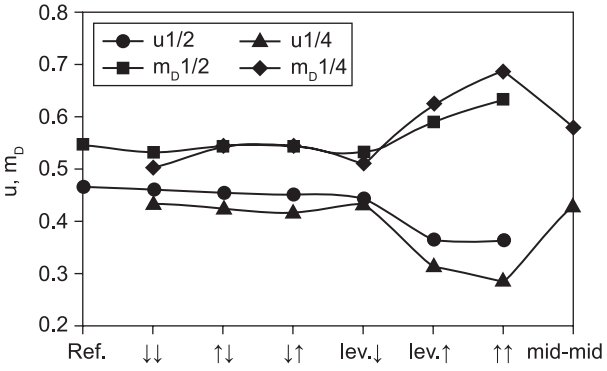

Figure 1. The dependence of the space utilization and fraction of dead space for sand dissolution on the input and output geometries of the channel <◄0; ↕0>.

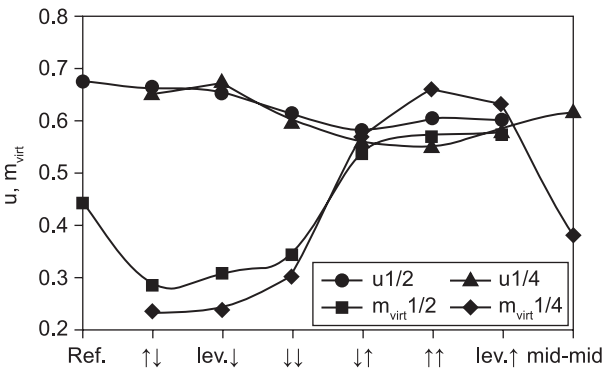

Figure 2. The dependence of the space utilization and fraction of virtual dead space for bubble removal on the input and output geometries of the channel <◄0; ↕0>.

The temperature gradients <◄4; ↕25> for bubble removal or <◄5; ↕25> for sand dissolution from previous works [14] were examined in more detail. The maximum of the dependence between the space utilization and the ratio ↕y/◄x was found at the mentioned combinations of temperature gradients in the previous work. The following two figures show the relations between the space utilization and the ratio of ↕y/◄x in the channel with the input and output of the type ↓↑ ¼ for sand dissolution and ↑↑ ¼ for bubble removal. The value of *u* at ↕y/◄x = 0 designates the isothermal case with the same input and output characteristics, and the value at ↕y/◄x = ∞ is the corresponding case with the pure transversal temperature gradient.

To verify the analogy between the full-size input–output and cases with the input and output geometries examined here also for disadvantageous cases, four additional cases were calculated, involving such with

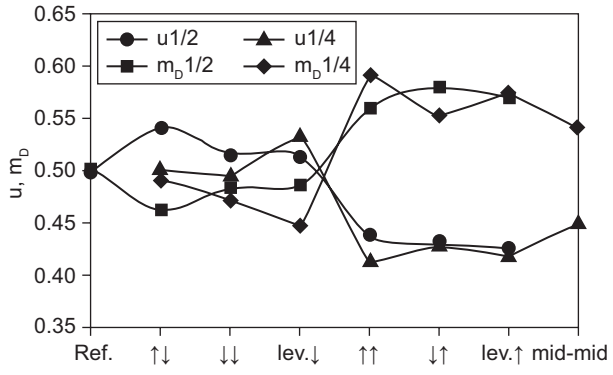

Figure 3. The dependence of the space utilization and dead space for sand dissolution on the input and output geometries of the channel <◄0; ↕25>.

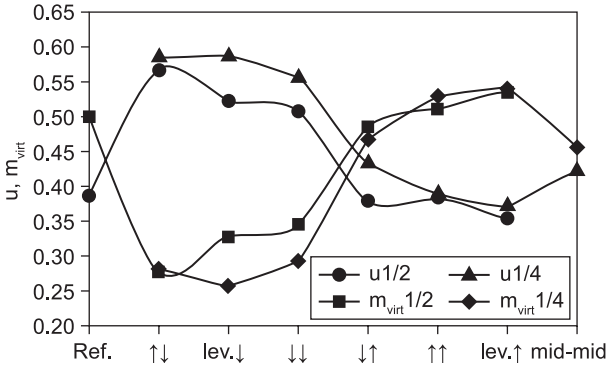

Figure 4. The dependence of the space utilization and fraction of virtual dead space for bubble removal on the input and output geometries of the channel <◄0; ↕25>.

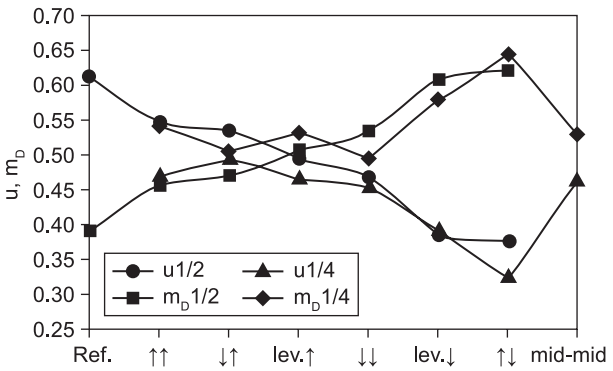

Figure 5. The dependence of the space utilization and fraction of dead space for sand dissolution on the input and output geometries of the channel <◄5; ↕25>.

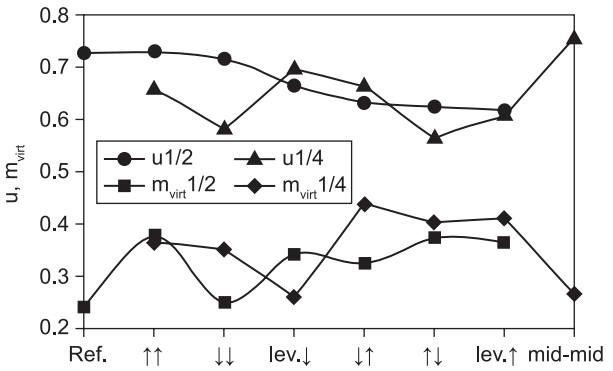

Figure 6. The dependence of the space utilization and fraction of virtual dead space for bubble removal on the input and output geometries of the channel <◄4; ↕25>.

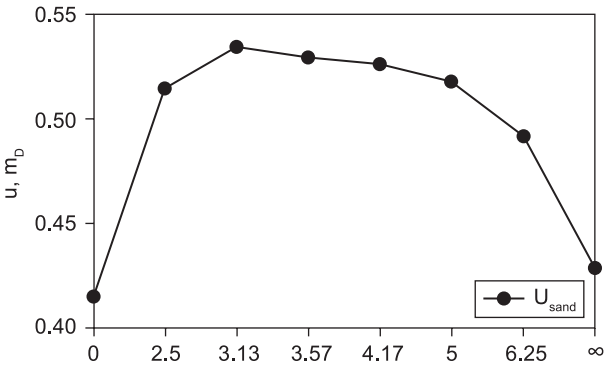

Figure 7. The dependence of the space utilization for sand dissolution on the ratio of ↕y/◄x. y is the value of the transversal temperature gradient and x the value of the longitudinal one.

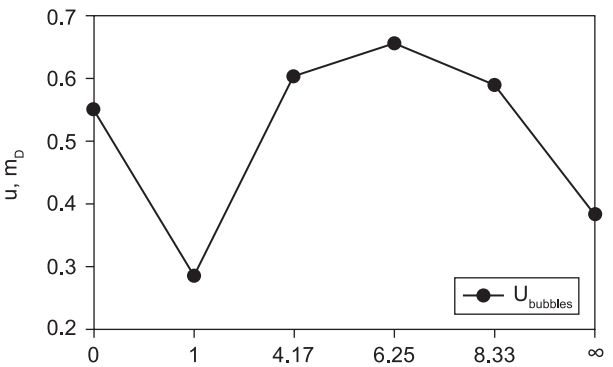

Figure 8. The dependence of the space utilization for bubble removal on the ratio of ↕y/◄x.

comparable values of the transversal and longitudinal temperature gradient, namely cases <◄25; ↕25> and <►25; ↕25> in the ↑↑ ¼ channel for both sand dissolution and bubble removal. The results are summarized in Table 1.

Table 1. The space-utilization values and appropriate dead spaces of the selected cases which were originally (in the reference case with full-size input and output) characterized by low space-utilization values.

Process	Temp. cond.	In/Out	Dead space	Space util.
Sand diss.	<◄25; ↕25>	↑↑	m_D = 0,7608	0.2580
Sand diss.	<►25; ↕25>	↑↑	m_D = 0,9020	0.0316
Bubble rem.	<◄25; ↕25>	↑↑	m_{virt} = 0,7802	0.2875
Bubble rem.	<►25; ↕25>	↑↑	m_{virt} = 0,8170	0.1376

DISCUSSION

The main results summarized in Figures 1-6 provide an overview of the relation between the input/output characteristics and the space utilization. The space-utilization values are plotted here against the input and output combinations to facilitate their visual appreciation. Besides the mentioned values, the values of m_D for sand dissolution and m_{virt} for bubble removal have been presented, because the values of both dead spaces significantly affect the resulting space utilization. Beneficial flow arrangements were applied [12-13], namely the pure transversal circulation flow - evoked by the transversal temperature gradient - and its combination with the small positive longitudinal temperature gradient (with a higher temperature at the output). The isothermal case was applied as the temperature reference case and the case characterized by full-size input and output as the geometry reference case (in the Figures designated by *Ref.*).

The results have generally shown that the character of the output plays a more important role in comparison with the input characteristics.

If the sand particles are dissolved at a constant temperature (the temperature reference case), the cases with bottom output provide mostly higher space-utilization values (see Figure 1) when compared to the top output, with the values being close to the case of full input and output. The reason for the lower u values in the case of top output is that some particles leaving the melt by the top output move too quickly close to the level, which results in the growth of the fraction of dead space, m_D (see Figure 1). The area fraction of the input and output (1/2 or 1/4) does not play any decisive role, but the values corresponding to the smaller input and output are slightly lower. The case of central input and output also shows good space-utilization values as the space output is relatively far from the level.

If the pure transversal circulations are introduced by the transversal temperature gradient; the best space-utilization values are shown by the cases with bottom output as well (see Figure 3), being even higher than the reference case shows with full-size input and output. The reason for the good results obtained in the cases with bottom output is the same as in the previous case: relatively low values of m_D. Generally, the space-utilization values are higher here than those obtained for the isothermal cases presented in Figure 1. The space-utilization values in the cases with smaller input and output (1/4) show only a slight decrease in comparison with the cases characterized by half-size input and output.

The application of the small positive longitudinal temperature gradient did not provide the absolutely best results attained earlier for the fully open channel (u = = 0.614, see the reference case in Figure 5 and 6). In contrast with the previous case of the pure transversal circulations, the top exit has shown higher space utilization than the bottom one. The most probable reason for this behavior is the enhancement of the melt and particle forward flow close to the channel bottom by the evoked longitudinal circulation. This leads to higher values of the dead space, m_D. The comparison between the half and quarter input or output also shows slightly lower utilization values for the quarter size input and output. The results generally show that the cases with restricted input and output do not require the small positive longitudinal temperature gradient as was the case with the full size input and output. The application of the pure transversal temperature gradient appeared to be a sufficient condition for good space utilization.

The calculated reference value of the fully opened isothermal channel for bubble removal was 0.678 (theoretically 0.667). Bubble trajectories cross the streamlines and, consequently, the bubble behavior is assumed to be less dependent on the input and output position and size (see Figure 2). The best results in the isothermal channel range between 0.61-0.67, being almost the same for both half- and quarter-size input or output. They logically come from the cases with bottom output. The utilization values are mostly influenced by the value of the virtual dead space, m_{virt}. Both u and m_{virt} are plotted in Figure 2. When compared with sand dissolution, the result scatterings shown by the different inputs and outputs are smaller in the case of bubble removal.

The utilization values in cases characterized by a pure transversal circulation flow (i.e. with the transversal temperature gradient having been applied) are relatively low as shown in Figure 4. This fact is in agreement with the reference case of full-size input and output providing the value of 0.388. The best space-utilization values are around 0.59, coming logically from quarter-size bottom output. The utilization values are mostly determined by the values of the virtual dead space, m_{virt}, with the values of h_{virt} being around 1 for all of the cases.

If the small positive longitudinal temperature gradient is applied in addition to the transversal one, the utilization values become relatively high, namely 0.60–0.73 because of the reduced melt-flow velocity close to the glass level. The best value even slightly exceeds the reference value of 0.727, valid for full-size input and output. This is apparent from Figure 6. Thus, the combination of the transversal and small positive longitudinal temperature gradients achieves the best space-utilization values for both the full and restricted input and output.

The question arises whether the restricted inputs and outputs preserve the overall character of the dependence between the character of glass flow (given by the adjusted temperature gradients) and space utilization, presented in [12-13]. Two additional cases were therefore calculated with a relatively high positive and negative longitudinal temperature gradient of 25°C/m, for quarter-size input or output and for both processes. The mentioned temperature distributions represented the cases with low space utilization as referred to in [12-13]. The new space-utilization values for the sand dissolution and bubble removal calculated in this work were low in both cases as well, which is evident from Table 1. The high values of dead spaces, namely m_D and m_{virt}, are typical for both the previous and present calculations.

In our previous work, the optimum space utilization was indicated at the defined ratio between the values of the transversal and longitudinal temperature gradient (the highest optimum values were found at the transversal temperature gradient of 25°C, see [14], Figures 5 and 6). Several values of the ratio ↕y/◄x (with the transversal temperature gradient being 25°C/m) were applied in this work to find the position of the optima and their possible shifting for the restricted input and output (to ¼) and for both processes. The results are plotted in Figures 7 and 8. Whereas the position of the optimum case for bubble removal remained roughly preserved as compared to the reference case with full-size input and output (the optimum value at ↕y/◄x = 6,25), the optimum space-utilization value for dissolution was shifted from ↕y/◄x = 5 to 3.13, with the differences in u however being small. The results show that the main tendencies of the relation between the melt flow character and space utilization were preserved.

CONCLUSION

The practical application of the results requires an implementable design of the melting channel. The original model channel with a full-size frontal input and output did not meet these conditions entirely. The simple and feasible inputs and outputs were tested in this work under previously-ascertained beneficial melt-flow conditions to verify the relation between the calculated space utilization and the different types of inputs and outputs. The results have shown that the main tendencies in the mentioned relation were preserved under the new conditions even though the numerical space-utilization values showed slight changes. Generally, the marginally better space-utilization values for the dissolution process were achieved in the case of the pure transversal circulations in the space (evoked by the transversal temperature gradients). The location of the input did not play any substantial role and the bottom exit proved to have better results than the upper one. The arrangements with transversal circulations and bottom exit seem to be the best variant of boundary conditions for the separate dissolution spaces. The optimal conditions of the bubble separation process were characterized by the combination of the transversal and small positive longitudinal temperature gradients in conjunction with the original full-size input and output. The mentioned conditions also evoked predominantly transversal circulations. The bottom output showed better results in comparison with the upper one. In most cases, the space-utilization values reduced with the decreasing size of the input and output in the range between the full size and the quarter size of frontal walls. The differences were generally small. The space-utilization values in favorable cases were close to the best ones achieved for the original full-size input and output arrangement.

Should both processes be implemented in one space, a compromise between the conditions has to be arranged in the space. The combination of transversal glass circulations – evoked by the transversal temperature gradient – and the small positive longitudinal temperature gradient meets the requirements of both processes (in conjunction with the original full-size input and output). The upper exit is then the compromising condition for both processes, and the sizes of the input and output between one half and one quarter of the full front walls proved to be favorable for further applications.

Acknowledgement

This work has been conducted with the financial support of specific university research (MSMT No. 21(2010)), is part of Project No. 2A-1TP1/063, "New glass and ceramic materials and advanced concepts of their preparation and manufacturing", implemented with the financial support of the Ministry of Industry and Trade, and Institutional Research Plan Proposal No. Z40320502, "Design, synthesis and characterisation of clusters, composites, complexes and other compounds based on inorganic substances; mechanisms and the kinetics of their interactions".

References

1. Simonis F., de Waal H., Beerkens R.: Collected Papers XIV. International Congress on Glass, Vol. III, pp. 118-127, New Delhi, India 1986,.
2. Beerkens R.: Ceramics-Silikáty *52*, 206 (2008).

3. Plumat E.: Glass Ind. *54*, 22 (1973).
4. Anon H.: Glass Ind. *69*, 19 (1988).
5. Barton J.L.: Collected Papers XVI International Congress on Glass, Vol. 1, pp. 165-184, Madrid, Spain 1992.
6. Noiret R. et al.: French Patent 2 550 523 (09.08.83).
7. Martlew D.: Glass melting. European Patent 0 403 183 (13.06.89).
8. Trevelyan R.E.: Glass melting. European Patent 0 403 184 (13.06.89).
9. Cozac D. et al.: Glass melting furnace. US Patent 5 078 777 (29.04.88).
10. Němec L., Jebavá M.: Eur. J. Glass Sci. Technol. A *47*, 68 (2006).
11. Němec L., Jebavá M., Cincibusová P.: Ceramics-Silikáty *50*, 140 (2006).
12. Němec L., Cincibusová P.: Ceramics-Silikáty *52*, 240 (2008).
13. Němec L., Cincibusová P.: Ceramics-Silikáty *53*, 145 (2009).
14. Němec L., Cincibusová P.: Sklář a keramik *60*, 1 (2010). (in Czech)
15. Schill P.: Proceedings of the 2nd International Seminar on Mathematical Simulation in the Glass Melting, pp. 102-116, Vsetín-Horní Bečva , Czech Republic, May 17-19 1993.